Deformation Rates of Polycrystalline Ice

Howard B. DILLON and O. B. ANDERSLAND
Department of Civil Engineering, Michigan State University, East Lansing, Michigan, U. S. A.

Abstract

The results of a series of creep tests at constant stress and several constant strain rate tests performed on cylindrical polycrystalline ice samples are reported. Experimental creep data and creep data available in the literature are analyzed in terms of the rate process theory assuming that one mechanism of deformation predominates. Best fit curves are adapted to the data at three temperatures using octahedral shear stresses and octahedral shear strain rates. High and low stress regions are approximately defined by strain rates greater or less than 10^{-5} per minute, respectively.

For low stresses, the analysis gives a value of 11.44 kcal/mole for the heat of activation. This agrees with the self-diffusion energy of 11 kcal/mole obtained approximately from the melting temperature by Dorn (1959). The experimental value for the entropy of activation equals −36.1 cal/mole/^{0}K. A combination of the experimental values for heat and entropy of activation gives a free energy of activation equal to about 21 kcal/mole for the low stresses and the temperature range under consideration. At higher stresses larger values for the free energy of activation are obtained, indicating a possible stress dependence. Flow volumes ranging from 2.5×10^7 to 5.3×10^7 cubic angstroms indicate that boundaries of ice grains or slip along basal planes of single ice crystals are probably involved in the creep process. Experimental creep data exhibit a discontinuity in the vicinity of −10 to −14°C in that faster creep rates are observed for the same stress at a colder temperature.

I. Introduction

Deformation and flow of polycrystalline ice results from shear strain occurring at each point in the ice mass. The amounts of shear strain depend on the relative rates at these different points. In order to calculate or predict the amount of deformation one must know the relationship between creep rate, stress, temperature, and structure. The considerable amount of information available in the literature (Glen, 1955, 1958, 1963; Butkovich and Landauer, 1959, 1960; Jellinek and Brill, 1956; Nakaya, 1958; Higashi, 1959; Tegart, 1964) contributes much in describing the behavior of ice masses under the action of stress.

The shape and orientation of individual crystals markedly influence deformational properties. Columnar ice crystals with parallel optic axes behave in a manner similar to that of single crystals. A random crystalline orientation gives decreasing creep rate which with time usually steadies to a definite quasi-viscous rate. At higher stresses a reacceleration appears. Both the power law and hyperbolic sine relationships have been used to show the dependence of minimum creep rates on stress.

The flow law for ice must be one that covers the complete relation between the stress tensor and the strain-rate tensor. There is evidence that hydrostatic pressure does

not affect the flow rate (Rigsby, 1958). Hence, the variation of strain rate is expressed in terms of a stress deviator. Nye (1953) has assumed that this relationship is one between the octahedral shear stress and the octahedral shear strain rate, the principal strain rates being parallel and proportional to the corresponding principal stress deviators. Glen (1962) states that this assumption is valid only as long as the ice grains are randomly oriented. Ice may recrystallize in such a way as to produce a preferred orientation for the flow. Hence, different results may be expected if the direction or nature of the stress applied to the ice should change.

Temperature has a strong influence on the deformation and flow of ice, as shown by Voytkovskiy (1960). The flow rate decreased by a factor of 10 for a 15°C drop in temperature from the melting point. The rate process theory has shown promise in describing the influence of temperature on creep rates (Butkovich and Landauer, 1960; Glen, 1955; Kauzmann, 1941). The only report of a change of rheological behavior with temperature is the observation (Butkovich, 1954) that the hardness of ice single crystals becomes equal on surfaces parallel and perpendicular to the basal plane at −10°C. Above this temperature the (0001) plane is harder and below it is softer. This may imply that glide and some other mechanism vary differently with temperature. Experimental creep data reported here indicate that some change does take place in the vicinity of −10 to −14°C.

Practically no information is available on how the ice grains contained in frozen soil interstices influence the deformation and flow of frozen soils. Ice grains form when the water is sufficiently supercooled so that nucleation can take place in an interstice. For clay soils only part of the water freezes, with the amount dependent upon physicochemical characteristics of the clay mineral fraction. The ice grains formed may or may not be polycrystalline in nature. The random directions by which contact stresses from soil particles are imposed on the ice grains would indicate that flow must also occur in random directions. The overall effect of varied stress directions would indicate that these ice grains should behave in a manner similar to that of polycrystalline ice. With this in mind and knowing that contact stresses in soils are relatively high, the tests reported here were performed on polycrystalline ice samples. It may be possible to correlate the deformational behavior of polycrystalline ice with the deformational behavior of frozen soils. Results of an unpublished study (Akili, 1966) on frozen soil indicate that ice grains contained in the soil interstices do play a role in the creep behavior of a frozen clay soil.

This paper presents the results of a series of creep tests at constant stress and a few constant strain rate tests performed on cylindrical polycrystalline ice samples at several temperatures. Data available in the literature have been incorporated into the paper to give expressions, based on the rate process theory, describing the overall dependence of strain rate on stress and temperature for polycrystalline ice.

II. Method

In order to predict the deformation rates of polycrystalline ice, experimental data are needed on its temperature, stress, and structure dependence plus a theory which combines these factors into a usable form. Data available in the literature provide

Table 1. Summary of creep data on polycrystalline ice

Glen (1954) Uniaxial comp. data at −1.5°C		Higashi (1959) Hollow ice cyl. Hydrostatic pressure data at −4.2°C		Butkovich and Landauer (1959) Shear and uniaxial comp. data at −5.0°C		Butkovich and Landauer (1960) Uniaxial comp. data from −1.3 to −18.9°C		Halbrook (1962) Uniaxial comp. data at −4.0°C		Dillon (in preparation) Uniaxial comp. data at −10°C		Dillon (in preparation) Uniaxial comp. data at −14°C	
τ_{oct} psi	$\dot{\gamma}_{oct}$ min^{-1}	τ_{oct} psi	$\dot{\gamma}_{oct}$ min^{-1}	τ_{oct} psi	$\dot{\gamma}_{oct}$ min^{-1}	τ_{oct} psi	$\dot{\gamma}_{oct}$ min^{-1}	τ_{oct} psi	$\dot{\gamma}_{oct}$ min^{-1}	τ_{oct} psi	$\dot{\gamma}_{oct}$ min^{-1}	τ_{oct} psi	$\dot{\gamma}_{oct}$ min^{-1}
						at −1.3°C							
7.2	4.2×10^{-7}	5.8	3.82×10^{-7}	14.2	6.0×10^{-7}	1.42	7.8×10^{-8}	61.8	8.90×10^{-5}	94.5	2.47×10^{-5}	94.5	9.20×10^{-5}
11.6	1.14×10^{-6}	14.5	1.05×10^{-6}	142.0	6.0×10^{-4}	0.78	5.0×10^{-8}	71.4	4.07×10^{-4}	85.0	6.05×10^{-4}	118	1.34×10^{-4}
18.0	2.1×10^{-6}	29.0	2.86×10^{-6}			0.14	6.1×10^{-9}	92.5	2.63×10^{-4}	121	2.32×10^{-4}	118	4.72×10^{-4}
27.6	7.63×10^{-6}	36.2	7.65×10^{-6}			at −3.2°C		92.5	6.65×10^{-4}	107	9.27×10^{-5}	118	5.23×10^{-4}
30.6	1.2×10^{-5}	40.5	1.91×10^{-5}			1.42	6.20×10^{-8}	123.2	1.46×10^{-3}	139	2.36×10^{-3}	141	8.13×10^{-3}
43.5	8.0×10^{-5}	42.0	3.82×10^{-5}			0.78	3.46×10^{-8}	123.2	3.46×10^{-3}	138	6.12×10^{-4}	189	5.82×10^{-3}
66.0	1.91×10^{-4}					0.14	4.42×10^{-9}	142	7.64×10^{-3}	161	1.68×10^{-3}	189	1.03×10^{-2}
						at −5.15°C				180	1.06×10^{-3}	189	1.16×10^{-2}
						1.42	4.05×10^{-8}						
						0.78	2.06×10^{-8}						
						0.14	3.96×10^{-9}						
						at −13.8°C							
						1.42	2.04×10^{-8}						
						0.78	1.09×10^{-8}						
						0.14	1.76×10^{-9}						
						at −18.9°C							
						1.42	1.02×10^{-8}						
						0.78	6.55×10^{-9}						
						0.14	1.35×10^{-9}						

information for low and intermediate stresses at several temperatures. Information from a number of references is summarized in Table 1. Experimental results reported here provide more data in the stress region close to failure for several temperatures.

Most current theories for creep are predicated on the hypothesis that creep arises primarily from thermal activation of units of flow (a single molecule or groups of molecules) over a free energy barrier under the simultaneous action of an applied stress (Kauzmann, 1941; Schoeck, 1961). Butkovich and Landauer (1960) indicated that the rate process theory, which leads to a hyperbolic sine stress dependence, best describes their experimental results at low stresses. In this paper the rate process theory is considered over the full stress range.

Kauzmann (1941) gives the following expression for the steady state creep rate:

$$s = \sum_i \left[\frac{2\lambda_i kT}{L_i h}\right] \exp\left[\frac{-\Delta F_i^*}{RT}\right] \sinh\left[\frac{q_i A_i l_i \sigma}{kT}\right], \tag{1}$$

where s is the shear rate; λ is the distance in the shear direction moved by flow units relative to one another in the unit process; L is the distance between layers of units of flow; ΔF^* is the free energy of activation per mole; q is the stress concentration factor; A is the area of a unit of flow in the shear plane; l is the distance through which the shear stress acts in carrying the unit of flow from the normal to the activated state; σ is the macroscopically observed shear stress; k is Boltzmann's constant equal to 1.38×10^{-16} ergs per mole per °C; h is Planck's constant equal to 6.626×10^{-27} erg-second; R is the gas constant equal to 1.986 cal per mole per °C; and T is the absolute temperature. The sum is over all possible creep processes. If the different deformation mechanisms depend on one another so that none of them can occur without the others going on simultaneously, then the slowest one (usually with the highest activation energy) will be rate controlling (Schoeck, 1961). If the various mechanisms are independent and each of them can individually produce deformation, then the fastest one (usually with the smallest activation energy) will be rate controlling. The analysis in this paper is limited to one mechanism predominating. If more than one mechanism predominates, unreasonable values of certain creep parameters are to be expected. The octahedral strain rate ($\dot{\gamma}_{oct}$) and octahedral shear stress (τ_{oct}) are substituted for s and σ, respectively, in eq. (1) for the application of Kauzmann's general theory to the available data on polycrystalline ice.

III. Apparatus and Experimental Procedure

This section describes the apparatus and procedure used in obtaining experimental data in the high stress range at several temperatures.

Sample preparation. Distilled, de-ionized, and de-aired water was used in the preparation of the ice samples. An aluminum mold, similar to that used by Leonards and Andersland (1960), served to form the cylindrical ice specimens (1.4 in dia.×2.8 in length). Care was taken in filling the mold to prevent air mixing. The filled mold was then placed in a cold box, maintained at a temperature of -18 ± 2°C, and the water allowed to supercool. Samples were frozen at $-4\pm1/2$°C, by seeding with a crystal of ice. Nucleation and growth proceeded at a fairly rapid rate throughout the sample and after

approximately 12 hours the mold was covered with plastic sheeting to prevent sublimation of the ice.

After a period of two or three days the tops of the cylindrical samples were trimmed to a smooth surface, recovered with the sheeting, and allowed to remain in the mold until just before testing. Samples were slightly cloudy and a few small air bubbles could be seen in the samples. Densities were very close to that of clear ice (0.917 g/cm^3). Examination of thin sections under a microscope showed granular grains, the largest of which were approximately 1 to 2 mm in dimension. No columnar grains were observed. It was assumed that this manner of sample preparation gave reasonably polycrystalline ice specimens.

Creep tests. An ice sample was taken from the aluminum mold inside the cold box to minimize any melting. Friction reducers and lucite disks were placed on each end and two rubber membranes placed over each sample. Figure 1 shows schematically how ice specimens were protected inside a triaxial cell. The friction reducer consisted of a

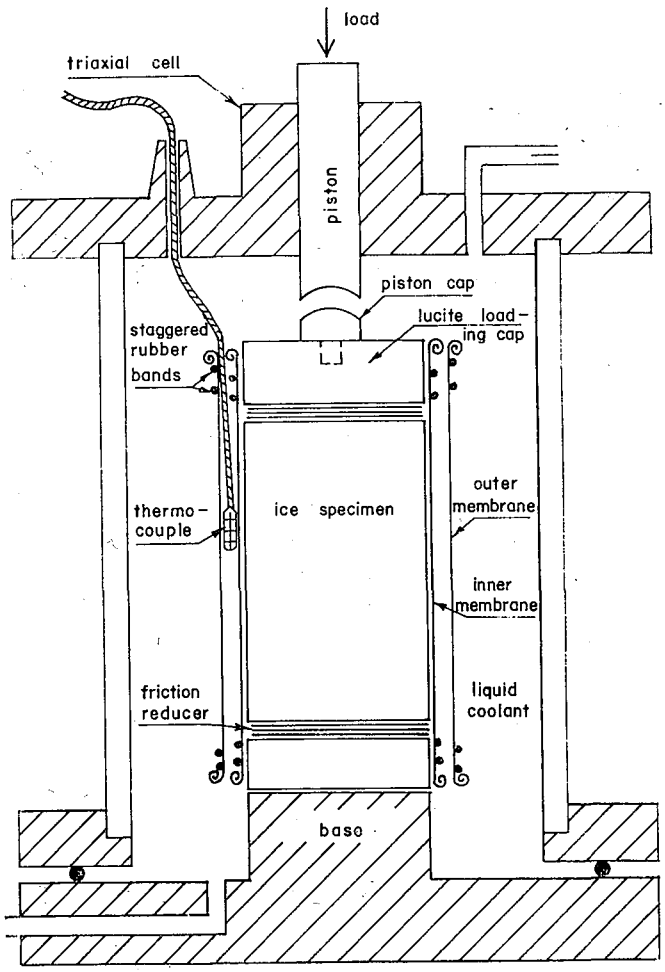

Fig. 1. Triaxial cell and ice sample prepared for test

perforated sheet of aluminum foil coated with a viscous mixture of silicone lubricant and finely powdered graphite covered by thin polyethylene sheets top and bottom. Isolation of the coolant liquid inside the cell from a surrounding coolant bath minimized sample temperature variations to less than ±0.05°C. Sample temperatures were measured by a copper-constantan thermocouple placed adjacent to the ice sample.

Axial loads up to the selected stress were applied to the specimen using an electrically powered mechanical system to lower dead weights. Upon deformation, a constant unit stress was maintained by adding lead shot to the dead weights to compensate for the small increase in sample area. Constant volume deformation was assumed in computing the required amounts of lead shot. Deformations were visually observed using a dial gage (0.0001 in accuracy) and recorded at appropriate time intervals.

Constant strain rate tests. Ice specimens were prepared in the same manner as for creep tests. Temperature control was achieved using a constant temperature coolant bath surrounding the triaxial cell. Axial deformation rates were controlled by an electrically powered mechanical load system with total loads observed on a proving ring (±5 lbs. accuracy). Strain rates were selected so as to permit comparison and possible correlation with observed steady state creep rates. Some difficulty was experienced in maintaining constant strain rates. They tended to increase after the initial peak load was reached, and stress tended to decrease. If the machine controls were adjusted, a constant strain rate was approximately maintained after reaching the peak load and the drop in stress was minimized.

IV. Results and Summary of Data

This section presents the experimental results and summary of data available in the literature. Two parts are included: creep tests and constant strain rate tests.

Creep tests. Typical creep curves at several temperatures and constant axial stress are shown in Fig. 2. All creep tests were performed in the high stress region on polycrystalline ice with the secondary creep data used in this paper tabulated in Table 1. Other data available in the literature have also been included. These data are plotted in Fig. 3, showing log octahedral shear stress versus log octahedral shear strain rate. The curves for the three temperatures (−1.5, −4.0 and −10.0°C) are "best fit" curves obtained using a hyperbolic sine chart, similar to the one developed by Nadai and McVetty (1943), and a plot of $\log_{10} \dot{\tau}_{oct}$ versus τ_{oct} for a constant temperature. The curves represent eq. (1) in the form below

$$\dot{\tau}_{oct} = \dot{\tau}_0 \sinh \frac{\tau_{oct}}{\tau_0}, \tag{2}$$

where

$$\dot{\tau}_0 = \frac{2\lambda kT}{Lh} \exp\left[\frac{-\Delta F^*}{RT}\right] \text{ and } \frac{1}{\tau_0} = \frac{qAl}{kT}.$$

The high and low stress regions are approximately defined by strain rates greater or less than 10^{-5} per minute, respectively. Strain rates are not well defined in the vicinity of $\dot{\tau}_{oct}$ equal to 10^{-5} per minute. Values of $\dot{\tau}_0$ and τ_0 for each temperature are given on Fig. 3 and in Table 2. For high stresses it was observed that $\dot{\tau}_0$ remains constant

for all three temperatures. Values of $1/\tau_0$ vary with temperature but for a given temperature are constant for both high and low stresses. At low stresses, values of $\dot{\gamma}_0$ vary slightly with temperature. A transition from one mode of creep behavior to another appears to separate the high and low stress regions.

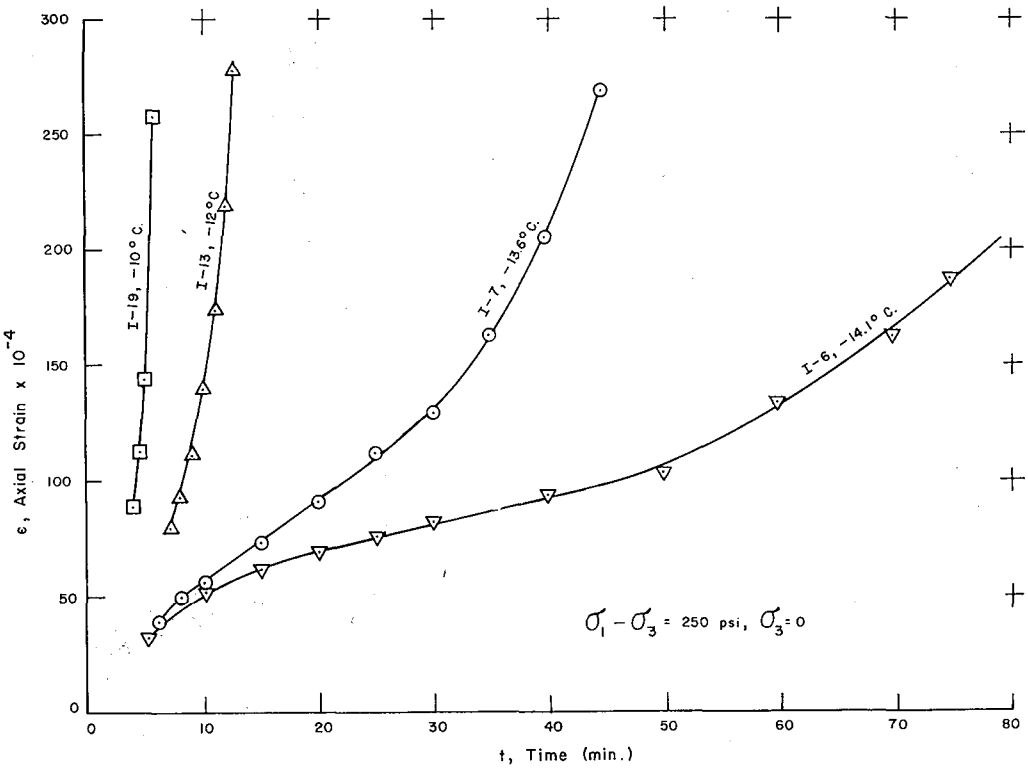

Fig. 2. Typical creep curves on polycrystalline ice

Table 2. Constants $\dot{\gamma}_0$, τ_0, and qAl

Temp. T (°K)	$1/T$ (1/°K)	$\dot{\gamma}_0$ (min^{-1})	$\dot{\gamma}_0/T$ (min^{-1}/°K)	τ_0 (psi)	qAl (Å^3)	B (°K/psi)
			Low stresses†			
263.16 (−10.0°C)	3.800×10^{-3}	3.75×10^{-7}	1.425×10^{-9}	20.0	2.58×10^{7}	—
269.16 (− 4.0°C)	3.715×10^{-3}	6.25×10^{-7}	2.320×10^{-9}	14.5	3.64×10^{7}	—
271.66 (− 1.5°C)	3.681×10^{-3}	7.50×10^{-7}	2.760×10^{-9}	10.0	5.32×10^{7}	—
			High stresses*			
263.16 (−10.0°C)	3.800×10^{-3}	1.00×10^{-6}	3.800×10^{-9}	20.0	2.58×10^{7}	13.18
269.16 (− 4.0°C)	3.715×10^{-3}	1.00×10^{-6}	3.715×10^{-9}	14.5	3.64×10^{7}	18.60
271.66 (− 1.5°C)	3.681×10^{-3}	1.00×10^{-6}	3.681×10^{-9}	10.0	5.32×10^{7}	27.20

† For stresses causing strain rates less than 10^{-5} per minute
* For stress causing strain rates greater than 10^{-5} per minute

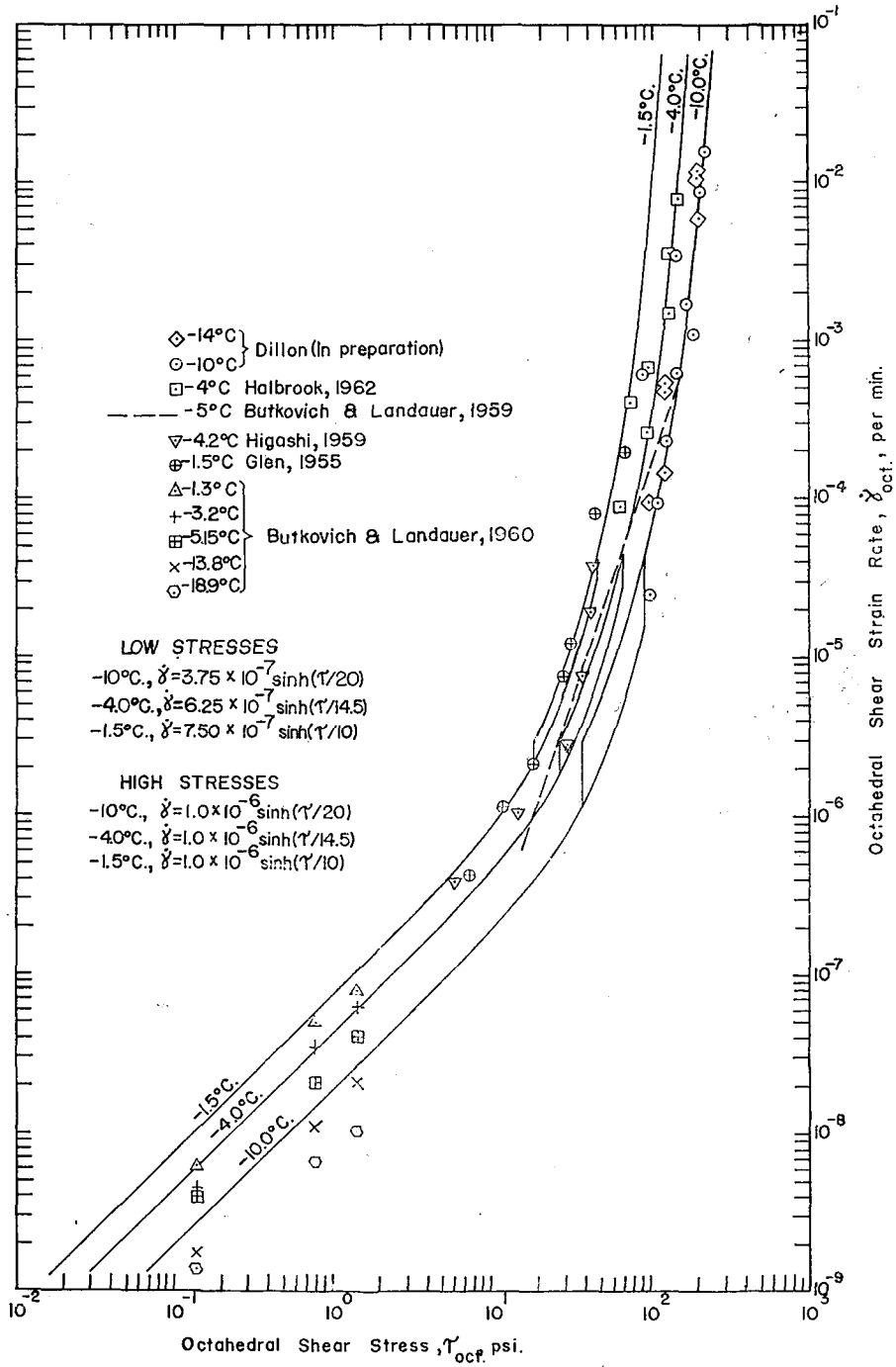

Fig. 3. Summary of creep data on polycrystalline ice

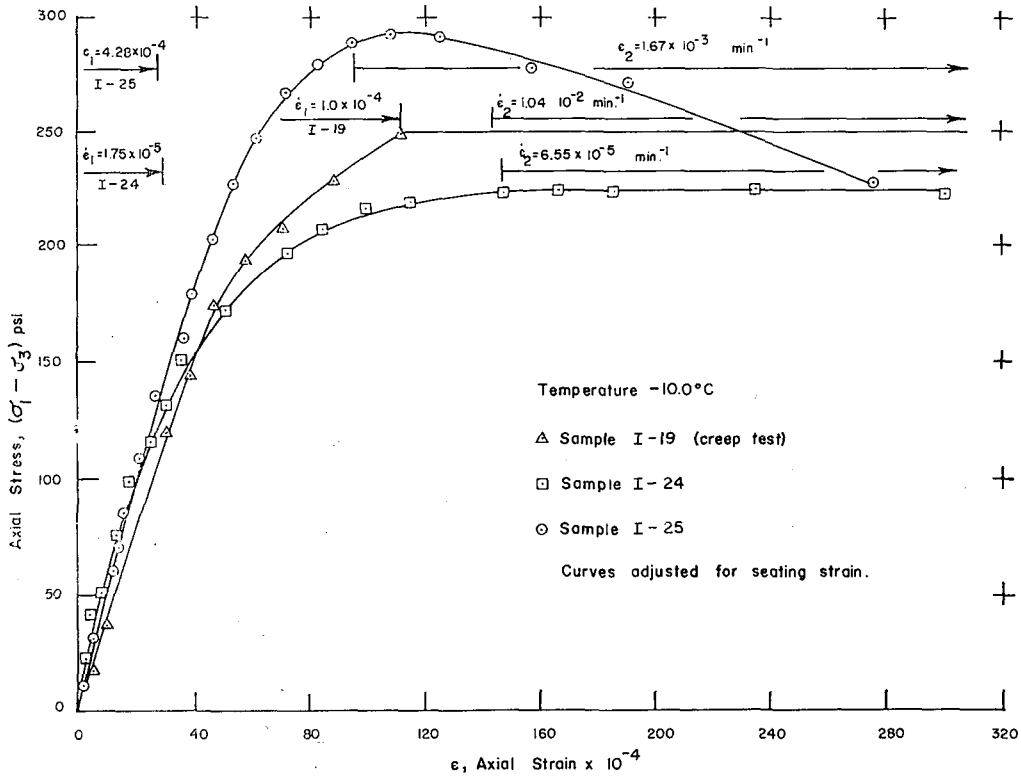

Fig. 4. Stress-strain curves for polycrystalline ice

Constant strain rate tests. Two stress-strain curves and the initial loading record for a creep curve are shown in Fig. 4. Peak axial stresses are reached close to 1 % axial strain. Difficulty was encountered with our equipment in maintaining a constant strain rate before and after reaching the peak axial stress. For those tests in which reasonably constant strain rates were maintained, the axial stress decreased very little after reaching the peak load (sample I–24). Similar stress-strain behavior was reported by Halbrook (1962). These limited data indicate a possible correlation between creep tests and constant strain rate tests provided accurate experimental control can be achieved.

V. Discussion

The application of rate process theory to the creep data for polycrystalline ice, summarized in Fig. 3 and Table 1, can be approached from the viewpoint presented by Kauzmann (1941) using eq. (1) in the form

$$\dot{\tau}_{\mathrm{oct}} = \frac{2\lambda kT}{Lh} \exp\left[\frac{-\Delta F^*}{RT}\right] \sinh\left[\frac{qAl}{kT}\tau_{\mathrm{oct}}\right]. \qquad (3)$$

Several methods are available for evaluating the unknown terms in eq. (3).

For low stresses the method utilized by Herrin and Jones (1963) on bituminous materials appears most suitable. Use is made of eq. (2) and the terms $\dot{\tau}_0$ and τ_0. From

thermodynamics ΔF^* equals $\Delta H^* - T\Delta S^*$ where ΔH^* is the heat of activation and ΔS^* is the entropy of the system. The term $\dot{\tau}_0$ may now be written

$$\dot{\tau}_0 = \frac{2\lambda kT}{Lh} \exp\left[\frac{\Delta S^*}{R}\right] \exp\left[\frac{-\Delta H^*}{RT}\right]. \tag{2 a}$$

Dividing through by T and taking the logarithm of this expression gives

$$\log_{10}\frac{\dot{\tau}_0}{T} = \log_{10}\left[\frac{2\lambda k}{Lh}\right] + \frac{\Delta S^*}{2.303R} - \left[\frac{\Delta H^*}{2.303R}\right]\frac{1}{T}. \tag{4}$$

A plot of $\log_{10}\dot{\tau}_0/T$ versus $1/T$ for three temperatures is shown in Fig. 5. The slope of this plot equals $\Delta H^*/2.303R$, giving ΔH^* equal to 11.44 kcal/mole. This value compares very favorably to 11 kcal/mole, reported by Dorn (1959) for the self-diffusion of ice.

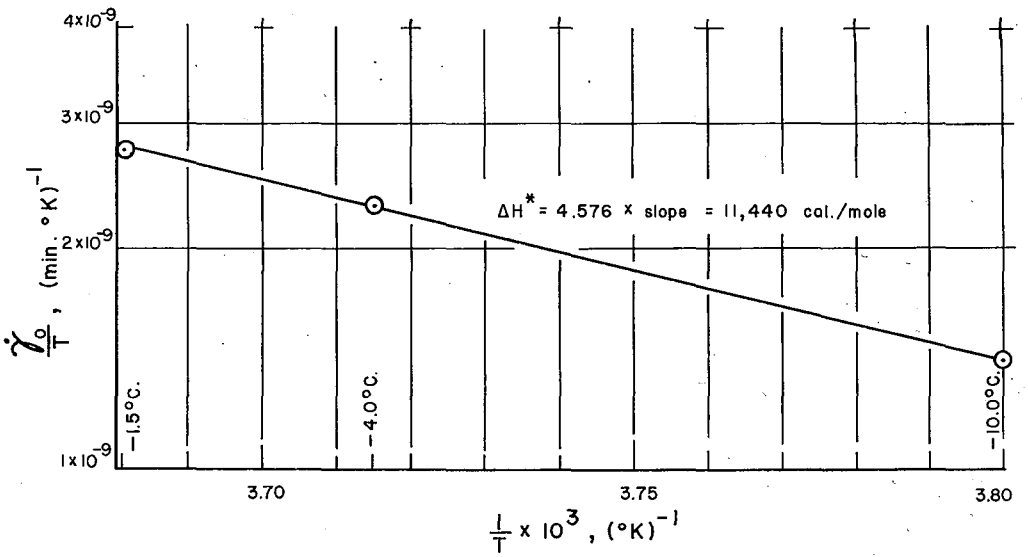

Fig. 5. $\text{Log}_{10}\dot{\tau}_0/T$ versus $1/T$ for polycrystalline ice at low stresses

If $2\lambda/L$ is assumed equal to unity, a reasonable value according to Kauzmann (1941), one obtains from the intercept (Fig. 5) a value of ΔS^* equal to -36.1 cal/mole/°K. Since $1/\tau_0$ equals qAl/kT, values of qAl may be calculated at the three temperatures. Values ranging from 2.5×10^7 to 5.3×10^7 cubic angstroms are obtained. This increase in flow volume (qAl) with temperature also occurs in metals (Kauzmann, 1941). The size of the flow unit indicates that boundaries of ice grains may be involved in the deformation process. Slip may also occur along the basal planes of single ice crystals (Nakaya, 1958; Gold, 1963). Using the thermodynamic relationship ΔF^* equal $\Delta H^* - T\Delta S^*$, one finds that ΔF^* equals 21 kcal/mole for the temperature range under consideration at these low stresses.

For high stresses sin h $[qAl/kT(\tau_{oct})] = 1/2$ exp $[qAl/kT(\tau_{oct})]$ such that eq. (3) becomes

$$\dot{\tau}_{oct} = \frac{\lambda kT}{Lh} \exp\left[\frac{-\Delta F^*}{RT}\right] \exp\left[\frac{qAl}{kT}\tau_{oct}\right], \tag{5}$$

for convenience let C equal $\lambda k/Lh$ and B equal qAl/k. Then dividing through by T,

eq. (5) may be written

$$\frac{\dot{\tau}_{oct}}{T} = C \exp\left[\frac{-\Delta F^*}{RT}\right] \exp\left[\frac{B}{T}\tau_{oct}\right]. \tag{6}$$

Taking the logarithm of eq. (6) gives

$$\log_{10}\left[\frac{\dot{\tau}_{oct}}{T}\right] = \log_{10} C + \frac{1}{2.303T}\left[B\tau_{oct} - \frac{\Delta F^*}{R}\right]. \tag{7}$$

The plot of $\log_{10}[\dot{\tau}_{oct}/T]$ versus $1/T$, shown in Fig. 6, gives curves with slope equal to $1/2.303\,[B\tau_{oct} - \Delta F^*/R]$. The curves in Fig. 6 are based on data presented in Fig. 3 for the three selected temperatures (−1.5, −4.0 and −10.0°C). Values for B are obtained from the slope of $\log_{10}\dot{\tau}_{oct}$ versus τ_{oct}/T (Fig. 7). The slope (Fig. 6) and B values for a particular stress and temperature permits the evaluation of ΔF^*. This has been done for a range of stresses and two temperatures with the results presented in Table 3. This method for evaluation of ΔF^* is limited to the high stress region where the hyperbolic sine approximates one-half the exponential and the accuracy of the curves on Figs. 3 and 6. More data are needed for intermediate temperatures which would improve the accuracy of Fig. 6.

One can also evaluate ΔF^* in the high stress range using eq. (2) and recognizing that $2\lambda/L$ should be close to unity. The value of $\dot{\tau}_0$ appears to be constant for the high stresses, as shown in Fig. 3. Equation (2) gives values for ΔF^* close to 25.5 kcal/mole,

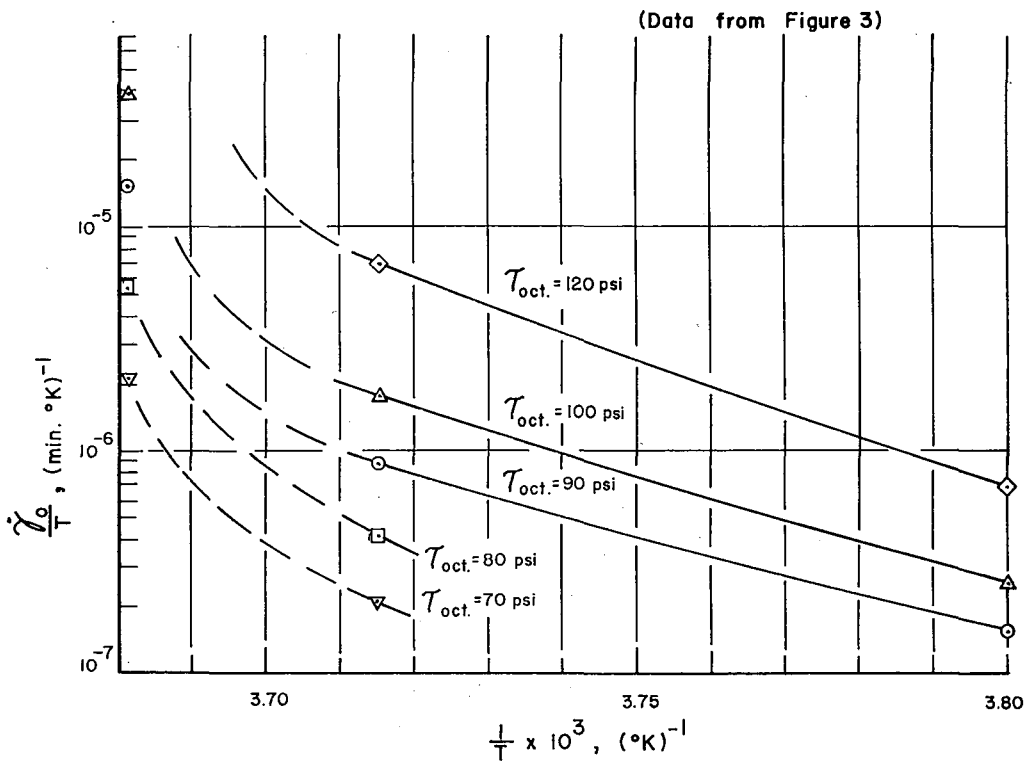

Fig. 6. $\text{Log}_{10}\,\dot{\tau}_0/T$ versus $1/T$ for polycrystalline ice

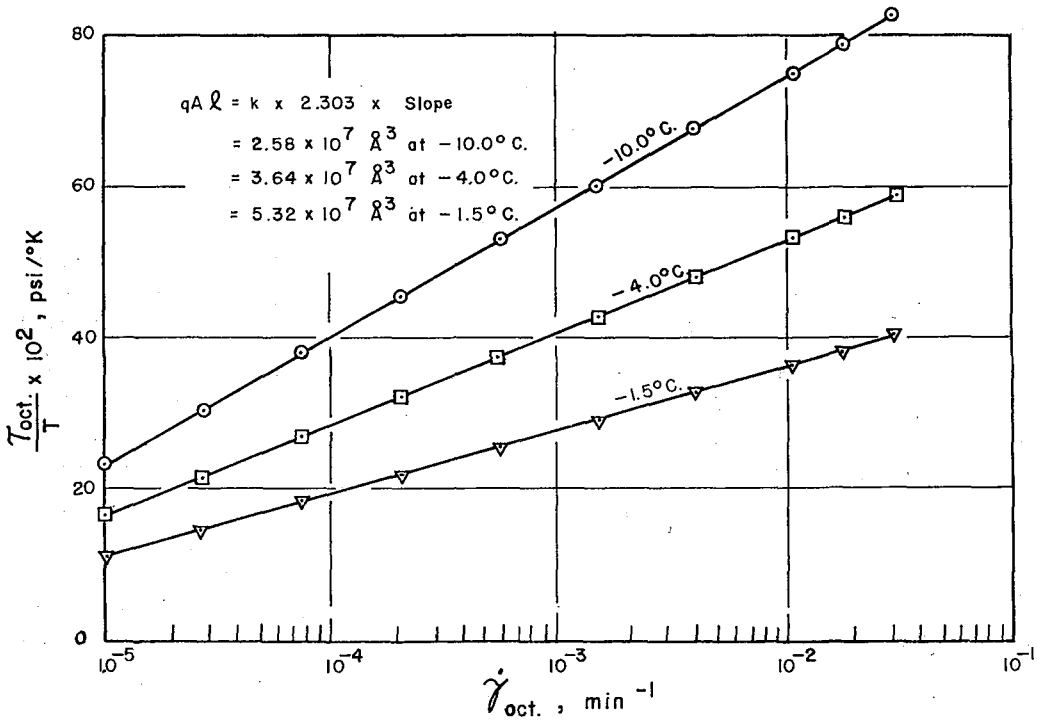

Fig. 7. $\text{Log}_{10}\dot{\tau}_{oct}$ versus τ_{oct}/T for polycrystalline ice (Data from curves of Fig. 3)

Table 3. Free energy of activation for polycrystalline ice at high stresses

Temperature, T (°C)	Shear stress, τ_{oct} (psi)	ΔF^* (kcal/mole)
−10.0	120	28.4
−10.0	100	22.8
−10.0	90	19.9
− 4.0	100	28.0
− 4.0	90	24.7

$\Delta F^* = (RqAl/k)\,\tau_{oct} - 4.576 \times$ (slope from Fig. 6)

not too different from values given in Table 3 for the preceding method. It appears that ΔF^* may be influenced to a small degree by stress and temperature. If the above values for ΔF^* are correct, presumably they would correspond to the predominating mechanism involved in accommodation cracking and larger distortions associated with high stresses (Gold, 1963).

The power flow law has not yet been used in this paper. A plot of $\log_{10}\dot{\tau}_{oct}$ versus $\log_{10}\tau_{oct}$ using data from Table 1 is presented in Fig. 8. Straight lines have been fitted by the least squares method through points corresponding to temperatures of −4.0, −10.0 and −14.0°C. One notes that the −14.0°C line crosses over the lines for warmer

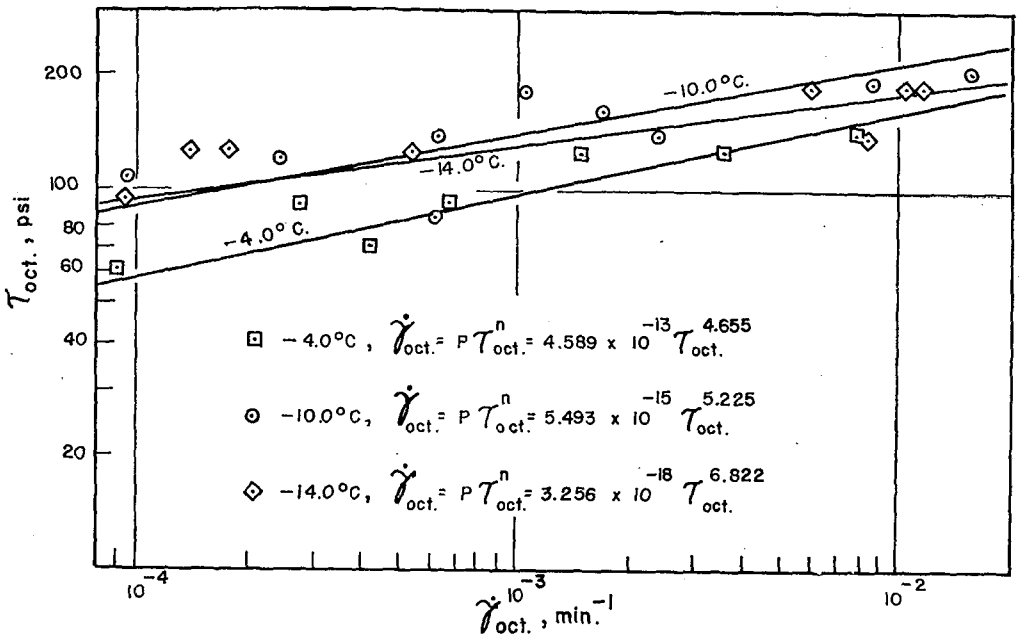

Fig. 8. Power law curves for creep data on polycrystalline ice

temperatures. Since the ultimate strengh of polycrystalline ice increases with decreasing temperatures, one would not expect this cross-over to occur. This must indicate some internal structural change in the ice between −10.0 and −14.0°C. The only reported change near this temperature is that of Butkovich (1954). It may be that certain other factors should be considered if the power law or the analysis used in this paper is to apply in this temperature range.

VI. Conclusions

The conclusions given below are based on the available data for secondary creep of polycrystalline ice and the methods of analysis used in this study.

1. A transition from one mode of creep behavior to another appears to separate the high and low stress regions at an octahedral shear strain rate close to 10^{-5}/min. The rate process theory seems to apply in both regions. Strain rates in the vicinity of $\dot{\tau}_{oct}$ equal to 10^{-5}/min are not well defined.

2. The predominating mechanism of deformation in the low stress range must be that of self-diffusion having an enthalpy of activation close to 11.44 kcal/mole. This agrees with the self-diffusion energy of 11 kcal/mole obtained approximately from the melting temperature by Dorn (1959).

3. A value of −36.1 cal/mole·deg was obtained for the entropy of activation based on the assumption that $2\lambda/L$ equals unity.

4. The computed size of the "activated flow volume" is on the order of 10^7 cubic angstroms indicating that boundaries of ice grains are probably involved in the creep process. Diffusion or accommodation cracking may take place primarily at grain

boundaries. Slip may also be occurring along the basal planes of single ice crystals (Nakaya, 1958; Gold, 1963).

5. There are indications that the free energy of activation may be a function of both the applied stress and temperature. Slightly higher activation energies were observed for higher stresses and warmer temperatures.

6. Comparison of creep data for temperatures at −10.0 and −14.0°C indicate some internal structural change in the ice. This is close to the temperature at which Butkovich (1954) reported a change in hardness of single ice crystals.

Acknowledgments

The research described in this paper represents a portion of the work supported by research grant number GP-1198 of the National Science Foundation, U.S.A.

References

1) AKILI, W. 1966 Stress Effect on Creep Rates of a Frozen Clay Soil from the Standpoint of Rate Process Theory, Unpublished Ph. D. Thesis, Michigan State University, East Lansing, Michigan.
2) BUTKOVICH, T. R. 1954 Hardness of single ice crystals. *SIPRE Res. Paper*, **9**, 1-9.
3) BUTKOVICH, T. R. and LANDAUER, J. K. 1960 Creep of ice at low stresses. *SIPRE Res. Rept.*, **72**, 1-6.
4) BUTKOVICH, T. R. and LANDAUER, J. K. 1959 The flow law for ice. *SIPRE Res. Rept.*, **56**, 1-7.
5) DILLON, H. B. Temperature Effect on Creep Rates of a Frozen Clay Soil, Unpublished Ph. D. Thesis (in preparation), Michigan State University, East Lansing, Michigan.
6) DORN, J. E. 1959 Creep and fracture of metals at high temperatures. *In* Proc. of Symposium of National Physical Laboratory, London.
7) GLEN, J. W. 1955 The creep of polycrystalline ice. *Proc. Roy. Soc.*, **A 228**, 519-538.
8) GLEN, J. W. 1958 The mechanical properties of ice. I. The plastic properties of ice. *Advances in Phys.*, **7**, 254-265.
9) GLEN, J. W. 1963 The rheology of ice. *In* Ice and Snow (W. D. KINGERY, *ed.*), M. I. T. Press, Cambridge, Mass., 3-7.
10) GOLD, L. W. 1963 Deformation mechanisms in ice. *In* Ice and Snow (W. D. KINGERY, *ed.*), M. I. T. Press, Cambridge, Mass., 8-27.
11) HALBROOK, T. R. 1962 Mechanical Properties of Ice, Unpublished M. S. Thesis, Michigan State University, East Lansing, Michigan.
12) HERRIN, M. and JONES, G. E. 1963 The behavior of bituminous materials from the viewpoint of the absolute rate theory. *Proc. Assoc. Asphalt Paving Tech.*, **32**, 82-101.
13) HIGASHI, A. 1959 Plastic deformation of hollow ice cylinders under hydrostatic pressure. *SIPRE* Res. Rept., **51**, 1-10.
14) JELLINEK, H. H. G. and BRILL, R. 1956 Viscoelastic properties of ice. *J. Appl. Phys.*, **27**, 1198-1209.
15) KAUZMANN, W. 1941 Flow of solid metals from the standpoint of the chemical-rate theory. *Trans. Amer. Inst. Min. Metall. Engnrs.*, **143**, 57-83.
16) LEONARDS, G. A. and ANDERSLAND, O. B. 1960 The clay water system and shearing resistance of clays. *In* Proc. ASCE Res. Conf. on the Shearing Strength of Cohesive

Soils, Univ. Colorado, 794–817.

17) NADAI, A. and MCVETTY, P. G. 1943 Hyperbolic sine chart for estimating working stresses of alloys at elevated temperatures. *Proc. Amer. Soc. for Testing Materials*, **43**, 735 pp.

18) NAKAYA, U. 1958 Mechanical properties of single crystals of ice. *SIPRE Res. Rept.*, **28**, 1–44.

19) NYE, J. F. 1953 The flow of ice from measurements in glacier tunnels, laboratory experiments, and the Jungfraufirn borehole experiment. *Proc. Roy. Soc.*, **A 219**, 477–489.

20) RIGSBY, G. P. 1958 Effect of hydrostatic pressure on shear deformation of single ice crystals. *J. Glaciol.*, **3**, 273–278.

21) SCHOECK, G. 1961 Theories of creep. Chap. 5. *In* Mechanical Behavior of Materials at Elevated Temperatures (J. E. DORN, *ed.*), McGraw-Hill Book Co., Inc., New York.

22) TEGART, W. J. M. 1964 Non-basal slip as a major deformation process in the creep of polycrystalline ice. *J. Glaciol.*, **5**, No. 38, 251–254.

23) VOYTKOVSKIY, K. F. 1960 Mekhanicheskiye svoystva l'da (Mechanical properties of ice). Acad. Sci. U. S. S. R.

Appendix-Notation

The following symbols have been adopted for use in this paper.

A	area of unit of flow in the shear plane
B	$\frac{qAl}{k}$
C	$\frac{\lambda k}{Lh}$
ε_1	axial compressive strain in triaxial compression
$\dot{\varepsilon}_1$	axial compressive strain rate in triaxial compression
ΔF^*	free energy of activation per mole
ΔH^*	the heat of activation per mole
ΔS^*	the entropy of activation per mole
h	Plank's constant $=6.626\times10^{-27}$ erg·sec
k	Boltzmann's constant $=1.38\times10^{-16}$ erg/mole·deg
L	distance between layers of units of flow
l	distance through which the shear stress acts in carrying the unit of flow from the normal to the activated state
λ	distance in shear direction moved by the flow units relative to one another in the unit process
P	a constant
q	a stress concentration factor
R	universal gas constant $=1.986$ cal/mole·deg
s	shear rate
T	absolute temperature
σ	applied normal stress
σ_1	axial stress in triaxial compression
σ_3	lateral stress in triaxial compression
τ_0	$\frac{kT}{qAl}$
τ_{oct}	octahedral shear stress
$\dot{\tau}_0$	$\frac{2\lambda kT}{Lh}\exp\left[\frac{-\Delta F^*}{RT}\right]$
$\dot{\tau}_{oct}$	octahedral shear strain rate